Geometrical optics model of Mie resonances

Günter Roll and Gustav Schweiger

Ruhr-Universität Bochum, Maschinenbau, Laseranwendungstechnik und Messsysteme, 44780 Bochum, Germany

Received March 4, 1999; revised manuscript received February 15, 2000; accepted March 15, 2000

The geometrical optics model of Mie resonances is presented. The ray path geometry is given and the resonance condition is discussed with special emphasis on the phase shift that the rays undergo at the surface of the dielectric sphere. On the basis of this model, approximate expressions for the positions of first-order resonances are given. Formulas for the cavity mode spacing are rederived in a simple manner. It is shown that the resonance linewidth can be calculated regarding the cavity losses. Formulas for the mode density of Mie resonances are given that account for the different width of resonances and thus may be adapted to specific experimental situations. © 2000 Optical Society of America [S0740-3232(00)00707-9]

OCIS codes: 080.0080, 290.0290, 080.1510, 290.4020, 140.4780, 260.5740.

1. INTRODUCTION

Optical resonances of dielectric spheres, so-called Mie resonances or morphology-dependent resonances,[1,2] have attracted considerable scientific interest in recent years. The strong resonant field enhancement within and near the surface of the sphere allows the observation of several nonlinear optical phenomena.[3,4] Resonance spectroscopy has proved to be a highly accurate tool in aerosol research.[5–8]

Mathematically these resonances represent electromagnetic eigenmodes of the sphere. Although (essentially) developed some decades ago,[9,10] the geometrical optics model of these modes seems not be widely known; several misleading statements can be found in the literature. The description of the interaction of electromagnetic radiation with matter by the concept of light rays is very appealing to human intuition. Additionally, compared with the rigorous theory, the equations obtained by a geometrical optics are more explicit than exact solutions; i.e., the physics is not buried in the properties of Bessel and Legendre functions. This allows one to derive approximations for several quantities in a relatively simple way.

Recently, the geometrical optics description of such modes was extended to polarization information.[11] The concepts were applied to dielectric cavities, and the coupling of external and internal fields was investigated. The occurrence of Mie resonances was predicted within a geometrical optics framework; formulas for positions, strength, and widths were given.[12] In contrast to previous work,[11,12] which dealt with the properties of eigenmodes in general, this paper focuses on resonant states.

2. ELECTROMAGNETIC EIGENMODES OF SPHERES

Mie theory provides the rigorous treatment of the interaction of a plane wave with a dielectric sphere. In Mie theory all involved fields are expanded in spherical multipole waves (eigenmodes); in resonance one eigenmode of the sphere is strongly excited. Each multipole wave is characterized by its state of polarization (TE or TM) and two integers, which enter in Mie theory as separation constants. These integers are the mode number $l = 1, 2, \ldots$, which is connected to the total angular momentum of the mode by $|L| = [l(l+1)]^{1/2}\hbar \approx (l + 1/2)\hbar$, and the azimuthal mode number $m \leqslant l$, which is a measure for the z component of the angular momentum, $L_z = m\hbar$.[13]

Modes that have the same mode number l but differ in m are degenerate; i.e., they occur at the same size parameter $x = k_0 a = (2\pi/\lambda_0)a$ (a is the sphere's radius, k_0 is the wave number, and λ_0 is the wavelength of the illuminating radiation). If a sphere is illuminated by a plane wave, only modes with $m = 1$ are excited.[14] Each multipole exhibits an infinite number of resonances as a function of the sphere's size parameter. These resonances are labeled by the mode order v; the lowest order, $v = 1$, appears at the lowest size parameter. Since all azimuthal modes are degenerate, it is sufficient to specify only the mode polarization, the mode number, and the mode order to identify a resonant state. It is common to write $\mathrm{TE}_{l,v}$ or $\mathrm{TM}_{l,v}$. The first-order resonance of a given multipole occurs at a size parameter that is given roughly by $x_{l,1} \approx \Lambda/n$, where $\Lambda = l + 1/2$ and n is the sphere's refractive index. Resonances of order 1 can be extremely sharp; specific values depend strongly on the sphere's size and refractive index, but the theoretical linewidth can be on the order of 10^{-20} size parameters or less. With increasing mode order the resonances tend to broaden and there is only a limited number N of resonances, which are narrow enough to not overlap. Resonances of order N occur at $x_{l,N} \approx \Lambda$.

The resonance positions are solutions of a characteristic equation that is conveniently expressed in terms of Ricatti–Bessel and Ricatti–Neumann functions and their derivatives.[1,2] The Ricatti–Bessel functions $\mathcal{G}_l(x)$ are connected to the spherical Bessel functions $g_l(x)$ by $\mathcal{G}_l(x) = x g_l(x)$, which holds for any member of the family of spherical Bessel functions. Since Bessel functions may be regarded as fast oscillating (or strongly exponentially varying) functions, the derivative of any Ricatti–Bessel function may be approximated by $\mathcal{G}_l'(x) \approx x g_l'(x)$. Un-

der this assumption the characteristic equation for Mie resonances reads

$$\frac{j_l'(nx)}{j_l(nx)} - \alpha^2 \frac{y_l'(x)}{y_l(x)} = 0, \tag{1}$$

where the primes denote derivation with respect to x and $\alpha = 1$ for the TE case and $\alpha = n$ for the TM case.

3. GEOMETRICAL OPTICS MODEL OF MIE RESONANCES: RAY-PATH GEOMETRY

Consider Fig. 1, which shows a ray propagating in a plane cross section of a sphere. In the following we will refer to this plane as the orbit plane. Every plane that (a) contains the center of the sphere and (b) has a normal vector $\mathbf{n}$, which makes an angle of $\pi/2 + \arcsin(m/\Lambda)$ with the z axis, is an orbit plane. Two oppositely oriented conical surfaces are shown in Fig. 1. The common apexes are located at the center of the sphere, and the opening angle is $\vartheta_c = \arcsin(m/\Lambda)$. These surfaces are caustic surfaces of the manifold of orbit planes. Each orbit plane contains a continuous manifold of rays, which travel along the sphere's inner surface on a zig-zag-shaped path (Fig. 1 shows only one representative member of this manifold). Each ray is restricted to one specific orbit plane and is confined to an annular region, which is limited by the sphere's surface on the outer side and a caustic circle on the inner side; this is the orbit of the considered ray. The circular caustics of all orbit planes together form a spherical caustic surface. In the following we will refer to the spherical caustic simply as caustic, whereas we will use the term ϑ-caustic for the conical caustic.

Now we follow a ray in its orbit. It is convenient to introduce a plane polar (r, η) coordinate system in the orbit plane, and we describe the ray propagation by the r and η components of the wave vector. If we set the ray's angular momentum $|L| = |k_\eta|r\hbar$ equal to that of the mode $|L| = \Lambda\hbar$, one obtains $k_\eta = \pm\Lambda/r$. Further, since $k^2 = k_\eta^2 + k_r^2$, the radial component of the internal wave vector ($|\mathbf{k}_i| = nk_0$) reads

$$k_{ir} = \pm\frac{(n^2k_0^2r^2 - \Lambda^2)^{1/2}}{r}. \tag{2}$$

The caustic radius r_{ci} follows from the condition $k_{ir}(r_{ci}) = 0$ and is given by

$$r_{ci} = \frac{\Lambda}{nk_0}. \tag{3}$$

Analogous arguments concerning the z component of the light's angular momentum yield the φ component of the wave vector $k_\varphi = \pm m/(r\sin\vartheta)$. The ϑ component readily follows from $k_\vartheta^2 = k^2 - k_r^2 - k_\varphi^2 = k_\eta^2 - k_\varphi^2$. Note that k_ϑ is zero for $\sin\vartheta = \sin\vartheta_c = m/\Lambda$, which mathematically reflects the fact that the cones mentioned above represent caustics.

At the caustics the associated wave-vector component is zero ($k_r(r_{ci}) = 0$, $k_\vartheta(\vartheta_c) = 0$) and becomes imaginary for $r < r_{ci}$ and $\sin\vartheta < \sin\vartheta_c$. Thus the caustics do not represent sharp field boundaries but are the surfaces of transition from radiating (real wave vector) to evanescent (partially imaginary wave vector) fields. On touching a caustic, a ray undergoes a phase delay of $-\pi/2$.[15]

Note that the above derivation of the wave-vector components did not rely on the assumption that the refractive index is constant but only on spherical symmetry; thus a radial dependence of the refractive index, $n = n(r)$, would not change the above argumentation. Rays propagate along straight lines in homogenous media. However, if there is a refractive-index gradient the rays follow a bent curve. It is important to realize that the rays remain in their plane orbits if the gradient of the refractive index has only a radial component. If not mentioned explicitly, we assume a constant refractive index throughout this paper. However, in many cases it is not difficult to generalize the results to inhomogeneous media.

If we restrict ourselves to smooth and monotonic radial refractive-index distributions and assume that a unique radius r_{ci} exists, which fulfills

$$\Lambda = k_0 n(r_{ci}) r_{ci}, \tag{4}$$

in such a case r_{ci} remains the closest distance to the center of the sphere for all rays with angular momentum $\Lambda\hbar$.

The tangential unit vector $\mathbf{e}_t$ fulfills

$$\mathbf{e}_t = \frac{d\mathbf{r}(s)}{ds} = \frac{1}{ds}\begin{pmatrix} dr \\ r\,d\eta \end{pmatrix} = \frac{1}{nk_0 r}\begin{pmatrix} (n^2k_0^2r^2 - \Gamma^2)^{1/2} \\ \Lambda \end{pmatrix} = \frac{\mathbf{k}_i}{nk_0}, \tag{5}$$

and with $n_{ci} = n(r_{ci})$ and Eq. (4) the path of the ray can be expressed as

$$\eta(r) = \eta(r_{ci}) \pm r_{ci}\int_{r_{ci}}^{r} \frac{n_{ci}}{n}\frac{d\rho}{\rho[\rho^2 - r_{ci}^2(n_{ci}/n)^2]^{1/2}}, \tag{6}$$

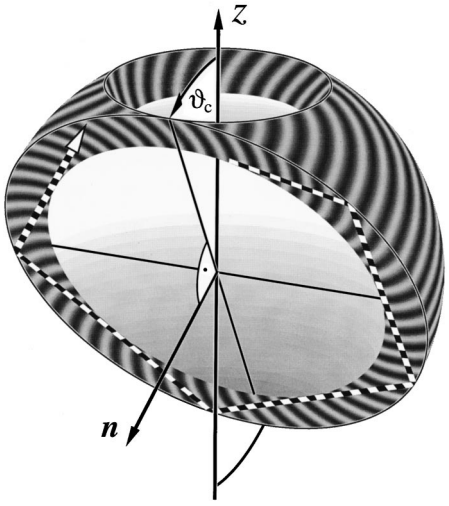

Fig. 1. Ray propagating within a sphere in the case of an eigenmode with mode number $l = 50$ and azimuthal mode number $m = 24$. The orbit of the ray is a plane annular region. The radius of the inner edge (a circular ray caustic) of this orbit is connected to the mode number by $nk_0r_{ci} = l + 1/2$. The orbit plane is inclined and makes an angle of $\pi/2 + \vartheta_c = \pi/2 + \arcsin[m/(l + 1/2)]$, where m is the azimuthal mode number, with the z axis. The incident plane wave is assumed to propagate in the z direction.

where n may be a function of the radial coordinate. In the case of constant refractive index ($n_{ci} = n$), the integral can be solved analytically, and Eq. (6) reads

$$\eta(r) = \eta(r_{ci}) \pm \arccos\left(\frac{r_{ci}}{r}\right), \tag{7}$$

which represents—as expected—a straight line.

4. RESONANCE CONDITION

A. Conditions for Self-Consistent Propagation

In the derivations of Section 3 the modulus of the wave vector was found; each component can be positively or negatively signed. For the complete description of a mode, $2^3 = 8$ waves have to be considered. The phase pattern shown in Fig. 1 was computed for $l = 50$; $m = 24$; and k_r, k_ϑ, and k_φ all positively signed (all components negatively signed, however, result in the same pattern; only the direction of propagation of the associated rays would be reversed). Each of the eight possible sign combinations represents a wave or a so-called ray congruence. When a ray propagating in its orbit hits the sphere's surface, k_r turns negative, whereas it turns positive when the ray touches the spherical caustic. On the other hand, k_ϑ turns positive (negative) at the north (south) pole ϑ caustic. The sign of k_φ never changes. From this perspective, in the course of propagation a ray repetitively changes the host wave, or host congruence. In this picture we do not assume that the phase fronts are fixed with the beam and change after each reflection but that the beam enters and leaves families of phase fronts at each reflection. Every ray encounters congruences of four different kinds (differing in the sign of k_r and /or k_ϑ). Whether all (infinitely many) host congruences of the same kind that a ray encounters in the course of propagation are in phase depends on the sphere's size. A state where all encountered congruences of the same kind are in phase represents a resonance.

The nonresonant and resonant cases are illustrated in Fig. 2. Each figure shows one complete round trip of a ray in its plane orbit. The phase of the ray (including the phase shifts at the caustic and at the surface) is shown as an alternating black and white shading. From the knowledge of the phase of the ray, the phase distribution of the wave (ray congruence) to which the ray belongs during the considered phase of propagation follows immediately. In each angular segment where the ray propagates radially inward or outward, an associated incoming or outgoing wave must be present; this wave fills the whole sphere. The phase distribution of the outgoing waves associated with the ray is shown in Fig. 2 in the associated angular segments. The phase of the ray and of the waves is shown in reversed shading to enhance the ray's visibility.

In the upper part of the figure the waves belonging to successive outward-propagating ray segments are out of phase, which can be recognized at the boundary between two angular segments where the mutual phase difference between two waves can be noticed. [The phase jumps must not been interpreted as discontinuities of the phase distribution but are a consequence of the (angular) piecewise representation, which has been chosen for reasons of illustration.] In contrast, in the lower part, where the sphere is slightly smaller, all waves that the ray encounters are in phase; the ray propagates resonantly. Only for particular distances between caustic and surface is the phase delay such that successive waves are in phase; i.e., a resonance is excited.

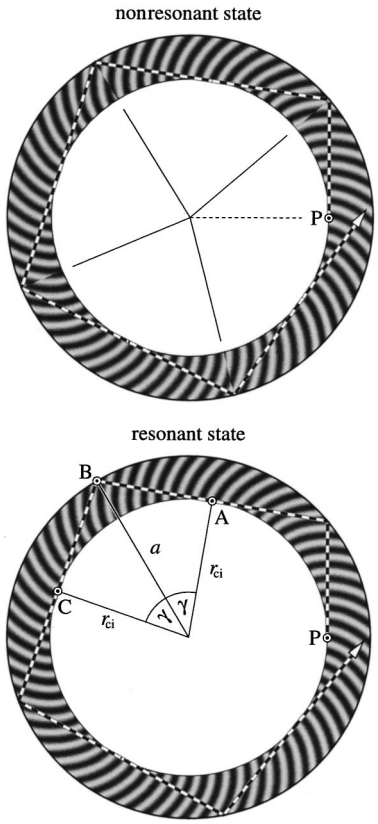

Fig. 2. Path of a ray within its orbit. In the upper part the size of the cavity is such that consecutive congruences of the same kind are not in phase; this represents a nonresonant case. In the lower part the cavity size is such that consecutive congruences are in phase; this state represents a resonance.

The phase delay of any two successive outward-propagating waves is given by the phase progress along the ray path ABC in Fig. 2 minus the angular phase progress of the wave between the points A and C, i.e., $2r_{ci}k_\eta\gamma$. We can therefore formulate the resonance condition as

$$nk_0\left[2(a^2 - r_{ci}^2)^{1/2} - r_{ci}2\arccos\left(\frac{r_{ci}}{a}\right)\right] + \delta_B - \frac{\pi}{2} = (\nu - 1)2\pi, \tag{8}$$

where δ_B is the boundary phase shift, $\pi/2$ represents the caustic phase shift and $\nu = 1, 2, \ldots$ is an integer, which can be identified as the mode order. For $\nu = 1$ the geometrical detour (the value in square brackets) is identically compensated by the phase shifts. We will give expressions for the boundary phase shift later.

To speak graphically, Eq. (8) is the necessary condition that in a representation such as Fig. 2 no discontinuity between the phase distribution in neighboring angular segments can be found.

Note that the size of the sphere in the upper part of Fig. 2 was chosen such that the phase difference of two successive waves equals $\pi/2$. This leads to the case that waves are in phase again after four reflections of the associated ray, i.e., after one round trip in the illustrated case. Obviously, this is not a sufficient condition for resonance, since every second wave is out of phase by π.

The propagation phase progress (i.e., the phase shifts at the boundary and at the caustic are not taken into account) along the ray $2nk_0(a^2 - r_{ci}^2)^{1/2}$ can also be written in integral form as follows:

$$2nk_0(a^2 - r_{ci}^2)^{1/2} = 2\int_A^B \mathbf{k}\cdot \mathrm{d}\mathbf{r} = 2\int_{r(A)=r_{ci}}^{r(B)=a} k_{ir}(r)\mathrm{d}r + 2\int_{\eta(A)}^{\eta(B)} k_\eta r\,\mathrm{d}\eta. \quad (9)$$

Introducing Eq. (9) into Eq. (8) and recognizing that

$$nk_0 r_{ci} = k_\eta r = \Lambda, \quad (10)$$

$$\int_{\eta(A)}^{\eta(B)} k_\eta r\,d\eta = \Lambda \arccos\left(\frac{r_{ci}}{a}\right), \quad (11)$$

we can write the resonance condition in the form

$$2\int_{r_{ci}}^{a} k_{ir}(r)\mathrm{d}r + \delta_B - \frac{\pi}{2} = (\nu - 1)2\pi. \quad (12)$$

The formulation of the resonance condition given by Eq. (12) allows an alternative interpretation of the resonance condition: In resonance the distance between caustic and surface is such that standing waves are excited by radially propagating waves that are reflected back and forth between caustic and surface.

For constant index of refraction, the above integral can be solved analytically. Using Eq. (2), one finds that phase propagation ϕ_r is

$$\phi_r(nk_0r) = \int_{r_{ci}}^{r} k_{ir}(\rho)\mathrm{d}\rho = (n^2k_0^2r^2 - \Lambda^2)^{1/2}\Lambda \arccos\left(\frac{\Lambda}{nk_0r}\right); \quad (13)$$

as expected, the first term in Eq. (8) equals $\phi_r(nx)$. A discussion of the accuracy of Eq. (12) is given below (see Fig. 4).

The only unknown in Eq. (12) is the boundary phase shift δ_B. If a plane wave with angle of incidence β is totally reflected at a plane interface, it undergoes a phase shift of[15]

$$\delta_B = -2\arctan\left(\alpha^2\frac{|k_{en}|}{k_{in}}\right) = -2\arctan\left[\alpha^2\frac{(\sin^2\beta - \sin^2\beta_{crit})^{1/2}}{\cos\beta}\right], \quad (14)$$

where k_{en} and k_{in} are the normal components of the wave vector in the external (thinner) and internal (thicker) medium, respectively; β is the angle of incidence in the thicker medium; β_{crit} is the critical angle of total reflection; and α depends on the polarization; $\alpha = 1$ in the TE case and $\alpha = n$ in the TM case. At least for large spheres ($x \gg 1$), it is reasonable to expect that the above expression is a good approximation of the boundary phase shift that a ray suffers at the spherical interface.

In the spherical case the radial wave-vector components have to be introduced into Eq. (14). For the internal medium this component was given in Eq. (2). For the external medium this component is given by $k_{er} = \pm(k_0^2 - k_\eta)^{1/2}$, where k_η is still given by $k_\eta = \Lambda/r$, since k_η is not a function of n and thus is continuous at the interface. We are interested primarily in cases where the internal rays are confined by total internal reflection, which implies that the radial wave-vector component is imaginary in the external medium, and write

$$k_{er}(r) = \pm i\frac{(\Lambda^2 - k_0^2r^2)^{1/2}}{r}. \quad (15)$$

Obviously, k_{er} is imaginary if $r < r_{ce} = \Lambda/k_0$, which means that the internal rays are totally reflected if $x < \Lambda$. This is consistent with the fact that only in this range is the angle of incidence

$$\sin\beta = \frac{r_{ci}}{a} = \frac{\Lambda}{nx} \quad (16)$$

larger than $1/n$, the critical angle of total reflection. If Eq. (2) and Eq. (15) or equivalently Eq. (16) is introduced into Eq. (14), one obtains

$$\delta_B = -2\arctan\left[\alpha^2\left(\frac{\Lambda^2 - x^2}{n^2x^2 - \Lambda^2}\right)^{1/2}\right]. \quad (17)$$

This boundary phase shift is zero for critical incidence and $-\pi$ for grazing incidence, independent of the polarization. For intermediate angles, δ_B depends on polarization.

Using Eq. (17), one can use Eq. (12) as an implicit equation to calculate the resonant size parameters $x_{l,v}$.

B. Connection to Mie Theory

For the range of interest, $k_0r < \Lambda < nk_0r$, the Debye expansions[16] of the spherical Bessel–Neumann functions read as

$$j_l(nk_0r) \approx \frac{\cos[\,\phi_r(nk_0r) - \pi/4]}{[nk_0r(n^2k_0^2r^2 - \Lambda^2)^{1/2}]^{1/2}}, \quad (18)$$

$$y_l(k_0r) \approx -\frac{\exp[-\psi_r(k_0r)]}{[k_0r(\Lambda^2 - k_0^2r^2)^{1/2}]^{1/2}}, \quad (19)$$

where $\phi_r(nk_0r)$ was given in Eq. (13) and $\psi_r(k_0r)$ is defined by

$$\psi_r(k_0r) = \int_{r_{ce}}^{r} |k_{er}(\rho)|\mathrm{d}\rho = (\Lambda^2 - k_0^2r^2)^{1/2} - \Lambda\left(\frac{\Lambda}{k_0r}\right), \quad (20)$$

where $r_{ce} = \Lambda/k_0$. Note that $\mathrm{d}\phi_r(nk_0r)/\mathrm{d}r = k_{ir}$ and $\mathrm{d}\psi_r(k_0r)/\mathrm{d}r = |k_{er}|$ were given in Eqs. (2) and (15). If Debye expansions (18) and (19) are now introduced into Eq. (1) and (a) the weak r dependence of the denomina-

tors in expansions (18) and (19) is neglected compared with that of the nominator and (b) the periodicity of the tan function is taken into account, one identically reproduces Eq. (12) using Eqs. (13) and (17).

C. Rays and Beams

In Subsection 4.B it was shown that the resonance positions predicted by the presented model are approximations to the results obtained from Mie theory. However, mathematically the agreement is restricted to cases in which the Debye expansions are good approximations of the spherical Bessel functions. The Debye expansions break down when the argument approximately equals the order, which means they break down at the ray caustics. We recognize that the model breaks down where geometrical optics breaks down anyway. With our model, however, we have a physical interpretation of this breakdown, namely, the breakdown of the concept of geometrical optics on ray caustics.[16]

In geometrical optics it is assumed that each beam is constructed by many local plane waves (rays) but that each point in space is intersected by only *one* local plane wave. It is known that multipole waves are composed of a spectrum of plane waves.[18] Thus, even if a single wave is considered, each point in space is intersected by a number of plane waves. But since all these plane waves are phase coupled, at each point in space there exists a direction with maximum phase change. The lines defined in this way are the rays of geometrical optics. Far away from the caustics this fact does not play an important role, and the ray treatment (Debye expansions) yield satisfactory results. Close to the caustics, however, where the character of the field changes from evanescent to oscillatory, the composition of the beam as a spectrum of plane waves is significant, since there is no sharp—but a more or less gradual—transition. The caustic is no sharp boundary; in a sense the caustic is "smeared." The situation is similar to that in which a spectrum of plane waves impinges on a plane interface under an angle close to the critical angle of total internal reflection; there, as well, there is no sudden change from light to darkness on the thinner side if the angle of incidence is varied gradually. The same happens when x approaches Λ. In the ray picture, if $x < \Lambda$ the ray is confined by total internal reflection (if the evanescent leakage is neglected), and if $x > \Lambda$ the ray is no longer trapped. In the beam picture, however, this change takes place gradually. Our model allows us to study this situation.

Since we know that the Debye expansion of the internal field [expression (18)] describes the field at the inner surface of the sphere for $nx \neq \Lambda$ with high accuracy, we can use it in Eq. (1) to study the case $x \approx \Lambda$. But instead of using the Debye expansion of the Neumann function (which breaks down if $x \approx \Lambda$), we will keep $y_l(x)$ and $y_l'(x)$ as they are in Eq. (1).

After introducing expression (18) and some rearrangements, Eq. (1) can be written similar to Eq. (12) but with the integral replaced by $\phi_r(nx)$ [as defined by Eq. (13)] and with the boundary phase shift term reading

$$\delta_{B,\mathrm{eff}} = -2 \arctan\left[-\alpha^2 \frac{y_l'(x)}{y_l(x)} \frac{x}{(n^2x^2 - \Lambda^2)^{1/2}} \right]. \quad (21)$$

This expression can now be interpreted as the boundary phase shift of the reflected beam, i.e., as the phase shift of the plane-wave spectrum. If x is not too close to Λ, the Debye expansion of $y_l(x)$, expression (19), is valid, and one has $-xy_l'(x)/y_l(x) \approx (\Lambda^2 - x^2)^{1/2}$, and Eq. (21) reduces to Eq. (17). But in contrast to Eq. (17), Eq. (21) also describes the situation for $x \approx \Lambda$ when not all plane waves that constitute the considered beam are totally reflected. Figure 3 shows the effective TE boundary phase shift $\delta_{B,\mathrm{eff}}$ for different values of l (main figure) and the boundary phase shift δ_B for a plane wave. The effect of polarization, i.e., TE or TM polarization of the waves, is also shown (inset). All plots are for $n = 1.5$. The dashed curve is the boundary phase shift of a plane wave with TE polarization. As can be seen, the angular region where the deviations between $\delta_{B,\mathrm{eff}}$ and δ_B have the same magnitude decreases with increasing l. There is always one angle where the deviation is zero, but the overall error clearly decreases, and one can extrapolate that for $l \to \infty$ the effective phase shift approaches that of a plane wave. This is in full agreement with the fact that the spectral width of the beams, which constitute the multipole waves, decreases with increasing l. The smaller the mode number l, the larger the spectral width and the farther from the critical angle the frustrated internal reflection can be observed.

Figure 4 shows the difference between the exact resonance position and that found with Eq. (12) by using $\delta_{B,\mathrm{eff}}$ and δ_B, respectively, for all 770 TE resonances with $75 \leqslant l \leqslant 150$ and $x < \Lambda$ as a function of the internal angle of incidence. Independent of the expression used for the boundary phase shift, the behavior and the sign of the error change with smaller mode order v, i.e., for grazing incidence. This is due to the breakdown of the ray picture near the internal caustic; mathematically, the reason is the breakdown of the Debye expansion of $j_l(nk_0r)$. However, close to the critical angle the error can largely be reduced (up to a factor of 10) by use of Eq. (21) for the boundary phase shift. Of course, using Eq. (21), which in a sense is a hybrid expression, may seem to

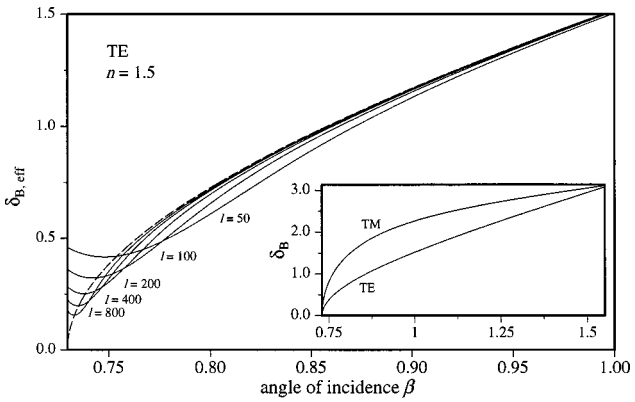

Fig. 3. Boundary phase shift $\delta_{B,\mathrm{eff}}$ as a function of the angle of incidence for different mode numbers l (solid curves) for the TE case and $n = 1.5$. The dashed curve shows the plane-wave–plane-boundary phase shift δ_B. The deviations between these curves can be understood if what are considered to propagate within the sphere are not rays but beams with a finite spectral width depending on l. The inset shows δ_B for the TE and TM cases for $n = 1.5$ and the full angular range.

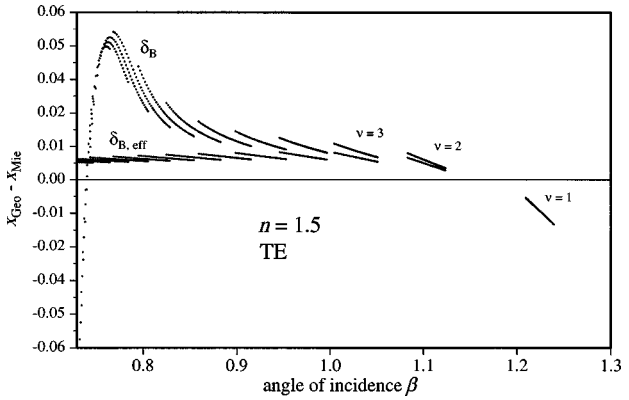

Fig. 4. Comparison of the resonance positions predicted by geometrical optics with exact positions for 770 TE resonances with $75 \leqslant l \leqslant 150$ and $x < \Lambda$. Resonances with identical mode order line up along smooth curves. Two sets were computed, with different expressions used for the boundary phase shift.

be artificial, since owing to the need to calculate $y_1(x)$ the computational effort is almost as high as that needed for the exact result. However, our objective for the preceding discussion was to provide a deeper understanding of the roots of the error in the transition region. We showed that the origin of this error is the oversimplified ray picture, which could be overcome by a more complete beam picture. Taking into account the partially frustrated total reflection reduces the error already to 0.005. However, even a position error of 0.005 may be too large to locate most resonances within their linewidths and Eq. (12) can serve only as an initial guess of the resonance position. Thus from a practical point of view it makes almost no difference which expression for the boundary phase shift, Eq. (17) or Eq. (21), is used.

5. MODEL PREDICTIONS

A. Resonance Positions

Equation (12) is a complicated function of the size parameter x and has to be solved numerically. However, for low-order resonances an explicit expression can be given. Rays that constitute low-order resonances, especially $v = 1$, circumnavigate within the sphere closely beneath its surface and are reflected under almost grazing incidence. In this case the boundary phase shift is approximately given by $-\pi$ and the internal caustic is almost as large as the sphere, $nx \approx \Lambda$. Using the angle γ, which is the complement angle of the ray's angle of incidence, given by

$$\cos \gamma = \frac{\Lambda}{nx}, \tag{22}$$

one may recast the resonance condition to read approximately

$$\Lambda(\tan \gamma - \gamma) = 3\,\frac{\pi}{4}. \tag{23}$$

Since γ is very small, we set $1/\cos \gamma \approx 1 + \gamma^2/2$ and $\tan \gamma \approx \gamma - \gamma^3/3$ and obtain

$$\tilde{x}_{l,1} = \frac{\Lambda}{n}[1 + 1.84\Lambda^{-2/3}] \tag{24}$$

as a first estimate of the resonance position. This result can now be used to refine our initial guess of the boundary phase shift; introducing Eq. (24) into Eq. (17), one finds the improved guess

$$\tilde{\delta}_B = -2 \arctan\left[\alpha^2\,\frac{(n^2 - 1)^{1/2}}{n}\,\frac{\Lambda^{1/3}}{1.92}\right] \tag{25}$$

For the boundary phase shift of a first-order resonance. After introduction of this result into resonance condition (12), and after a derivation analogous to that from Eq. (23) to Eq. (24), one finally obtains the expression

$$x_{l,1} = \frac{\Lambda}{n}\left\{\Lambda + 1.84\Lambda^{-2/3}\left[1 - \frac{2}{3\pi}(\pi + \tilde{\delta}_B)\right]\right\} \tag{26}$$

Since $\tilde{\delta}_B$ depends on polarization, the dependence of the resonance position on polarization is included in Eq. (26). For $l = 100$ the absolute error of Eq. (26) is on the order of 0.1 in size parameter in contrast to an error of approximately 5 size parameters for the simplest guess $x_{l,1} = \Lambda/n$.

B. Cavity Mode Spacing

A quantity of great practical interest is the cavity mode spacing or resonance distance. Two different kinds of spacings can be distinguished: (1) the distance between resonances of consecutive mode number but identical mode order $\Delta x_v = x_{l+1,v} - x_{l,v}$ and (2) the distance between resonances of identical mode number and consecutive mode order $\Delta x_l = x_{l,v+1} - x_{l,v}$.

In terms of ray propagation, Δx_v is the increase in resonator size necessary to keep the difference between the path ABC in Fig. 2 and the arc AC constant while the circumference of the caustic is increased by one wavelength. For large resonators ($x \gg 1$, $\Lambda \gg 1$) it is reasonable to expect that the difference in ray-path geometry (angle of incidence) for neighboring modes is not significant; in particular, we expect that the boundary phase shift will not be changed much. Mathematically this leads to the condition

$$\Delta\phi_r(nx) = \frac{\partial\phi_r(nx)}{\partial x}\Delta x_v + \frac{\partial\phi_r(nx)}{\partial l}\Delta l = 0, \tag{27}$$

where the increase in the mode number Δl is unity, $\Delta l = 1$. The above derivatives are easily evaluated with Eq. (13), and one gets

$$\frac{\partial\phi_r(nx)}{\partial x} = \frac{(n^2x^2 - \Lambda^2)^{1/2}}{x},$$

$$\frac{\partial\phi_r(nx)}{\partial l} = -\arccos\left(\frac{\Lambda}{nx}\right). \tag{28}$$

After some algebraic manipulations Chýlek's[19] well-known result

$$\Delta x_v = \frac{x}{\Lambda}\,\frac{\arctan[(nx/\Lambda)^2 - 1]^{1/2}}{[(nx/\Lambda)^2 - 1]^{1/2}} \tag{29}$$

is reproduced.

In quite the same way an expression for Δx_l can be derived. This resonance spacing is the change in particle size necessary to increase the phase difference between the ray propagating along *ABC* and the arc *AC* by 2π while keeping the circumference of the caustic constant (again we assume that the boundary phase shift is not affected). Mathematically this translates to

$$\Delta\phi_r(nx) = \frac{\partial\phi_r(nx)}{\partial x}\Delta x_l = \pi, \tag{30}$$

from which Probert-Jones's[20] result

$$\Delta x_l = \frac{x}{\Lambda}\frac{\pi}{[(nx/\Lambda)^2 - 1]^{1/2}} \tag{31}$$

is rederived.

C. Internal Energy Distribution

In the case of a resonance the electric field within the sphere is enhanced by several orders of magnitude. Since different modes occupy different mode volumes, it is possible to profile the chemical composition of spherical droplets.[5,6] Only modes with $(x < \Lambda)$ are confined by total internal reflection; thus it is not possible to probe a sphere more deeply than to a radial coordinate of a/n by resonance spectroscopy.

Of particular importance for spectroscopic applications is the knowledge of the radial position of the maximum of the angle-averaged internal field intensity (AAI), which is the location of probing. From Mie theory it is known that in the TE case the radial dependence of the AAI of each mode scales with the square of the associated spherical Bessel function, i.e., $j_l^2(nk_0r)$. With expression (18) this translates into the condition

$$\phi_r(nk_0r_{\max}) = \pi/4. \tag{32}$$

In the case of a TM mode the radial dependence of the AAI is a bit more complicated, but using relations (64)–(69) of a recent paper,[11] one can see that near the radial caustic $(k_r = 0)$, also in the TM case the AAI approximately scales with $\cos^2[\phi_r(nk_0r_{\max}) - \pi/4]$, thus leading to the identical condition.

Equation (32) can be solved pretty much the same way as was done for the derivation of Eq. (24). We just replace x by $k_0r_{\max}$ and get

$$\frac{r_{\max}}{a} \approx \frac{\Lambda}{nx}[1 + 0.885\Lambda^{-2/3}], \tag{33}$$

or equivalently $r_{\max} = r_{ci}[1 + 0.885\Lambda^{-2/3}]$. This result is in good agreement with numerical investigations[21] and is an improvement compared with the frequently used first-order estimate $r_{\max}/a = \Lambda/(nx)$.

D. Resonance Linewidth

In the case of a resonance, the internal energy as well as the scattered intensity exhibits a (more or less) sharp peak. If the effect of a small deviation from the resonance position on the above-mentioned quantities is investigated, the expression

$$\Delta x = \frac{2}{(n^2 - 1)px^2Y_l^2(x)}, \qquad p = \begin{cases} 1 & \text{for TE modes} \\ (\Lambda/x)^2 + (\Lambda/nx)^2 - 1 & \text{for TM modes'} \end{cases} \tag{34}$$

with $y(x)$ the Neumann function of order l for the width of the resonance, can been derived.[22,23] In the framework of geometrical optics, but using an analogous strategy, the authors and a colleague recently derived essentially the same result for the resonance linewidth.[12] In a sense, the above-mentioned strategy represents a direct approach, since the consequence of a variation of x is studied directly. In the following we give a different derivation of the above result, which is more closely related to the concept of light rays.

A dielectric cavity is inherently lossy, and it is common to define the characteristic time for the rise or decay of the mode energy $\Delta t = W/P_L$, where W is the mode energy and P_L is the energy loss per unit time. Since the size parameter $x = k_0a = (a/c)\omega$ can be understood as defining frequency ω, and since frequency and time domains may be connected by a Fourier transform, there is a close relation between the resonance linewidth Δx and the characteristic time[2]:

$$\Delta x\Delta t = x/\omega = a/c; \tag{35}$$

c is the vacuum speed of light.

It is not difficult to express the characteristic time in terms of ray propagation: Consider a pencil of light within the spherical cavity as shown in Fig. 5. Let this pencil carry a power of P, which means that the energy per unit length within this pencil is Pn/c. If the distance between two surface interactions is s, the pencil contributes with $W = Psn/c$ to the internal energy of the mode.

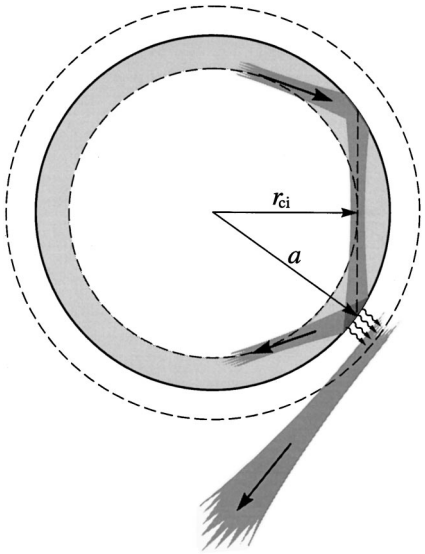

Fig. 5. Pictorial representation of the considered situation to derive an expression for the resonance width by means of cavity-loss arguments. A beam is (almost) totally reflected at the inner cavity surface. As a result of the evanescent leakage (tunneling, indicated by wavy arrows) a small amount of energy is coupled to the exterior and radiates away. This leakage ultimately limits the resonator quality factor.

On the other hand, the pencil continuously loses a power of $P_L = TP$, where T is the power transmission coefficient[24] to the exterior.

If Eq. (35) is now solved for Δx and $s = 2(a^2 - r_{ci}^2)^{1/2}$ is introduced, one obtains, after some rearrangements,

$$\Delta x = \frac{xT}{2(n^2x^2 - \Lambda^2)^{1/2}}. \tag{36}$$

The remaining task is to find an expression for the power transmission coefficient T. In order not to interrupt the discussion at this point, we simply give the result,

$$T = \frac{4(n^2x^2 - \Lambda^2)^{1/2}(\Lambda^2 - x^2)^{1/2}}{(n^2 - 1)x^2p}\exp[2\psi_r(x)], \tag{37}$$

with p as defined in Eqs. (34) and justify it later. If Eq. (37) is introduced into Eq. (36), one finally obtains

$$\Delta x = \frac{2(\Lambda^2 - x^2)^{1/2}}{(n^2 - 1)xp}\exp[2\psi_r(x)], \tag{38}$$

which is identical to Eqs. (34) if the spherical Neumann function is replaced by its Debye expansion [expression (19)]. Equation (38) was used successfully to derive expressions for the expansion order in Mie computations, which allow one to extract or remove certain features from calculated Mie spectra.[25]

The above formula predicts zero linewidth if $x = \Lambda$, which is not reasonable, since the size parameter $x = \Lambda$ marks the transition from efficient ray confinement by total internal reflection ($x < \Lambda$) to lossy refractively coupled internal and external fields; we thus expect broad resonances in this regime. The modification,

$$\Delta x = \Delta x_{trans}\exp[2\psi_r(x)], \tag{39}$$

where

$$\Delta x_{trans} = \frac{2.12\alpha^2}{(n^2 - 1)\Lambda^{1/3}} = \frac{2.12\alpha^2}{(n^2 - 1)x^{1/3}}, \tag{40}$$

is the linewidth at transition $x = \Lambda$, is more useful in such cases.[25]

To complete this section, we will give the derivation of Eq. (37). The Fresnel amplitude reflection and transmission coefficients are functions only of the wave-vector components normal to the interface, k_{en} and k_{in}, and the refractive index. The general expression for the transmission coefficient is

$$t_f = \frac{2\alpha k_{in}}{k_{in} + \alpha^2 k_{en}} = \frac{2\alpha(n^2x^2 - \Lambda^2)^{1/2}}{(n^2x^2 - \Lambda^2)^{1/2} + \alpha^2(\Lambda^2 - x^2)^{1/2}i}, \tag{41}$$

where we have expressed the radial wave-vector components by Eqs. (2) and (15); as before, $\alpha = 1$ in the TE case and $\alpha = n$ in the TM case. Using Eq. (41), we get the power transmission as

$$T_f = \left| t_f t_f^* \frac{k_{en}}{k_{in}} \right| = \frac{4(n^2x^2 - \Lambda^2)^{1/2}(\Lambda^2 - x^2)^{1/2}}{(n^2x^2 - \Lambda^2)/\alpha^2 + (\Lambda^2 - x^2)\alpha^2}. \tag{42}$$

Now it is time to think about the meaning of the above quantities. If a plane wave is totally reflected at a plane interface, the (net) power transmission into the thinner medium is zero although the amplitude and power transmission coefficients are not zero. The reason for this is that the field in the thinner medium is evanescent, i.e., at total reflection at the surface $x = 0$ it is given by $E_e(x) = t_f\exp(-|k_{ex}|x)$ in the thinner medium.[26] Since k_{ex} is constant, the external field is evanescent everywhere in the thinner medium, and the field decays asymptotically to zero with increasing distance from the interface.

At a curved interface the situation is different. The radial component,

$$k_{er}(r) = \frac{(k_0^2r^2 - \Lambda^2)^{1/2}}{r}, \tag{43}$$

of the wave vector is not constant in the exterior medium, and—what is especially important—it changes from being imaginary to being real at the external caustic, which is located at $r_{ce} = \Lambda/k_0$. At this radial position the field changes from being evanescent to oscillatory, and energy is radiated into space at this point. Relative to the electric field of the wave that is reflected totally at the sphere's inner surface, the field in the external medium is given by

$$E_e(r) = t_f\exp\left(-\int_a^r |k_{er}(\rho)|\mathrm{d}\rho\right). \tag{44}$$

At the external caustic the energy is radiated into space; we thus find the effective transmission coefficient to be

$$t = t_f\exp[\psi_r(x)], \tag{45}$$

where ψ_r as defined in Eq. (20) was used. In contrast to a plane interface, at curved interfaces the evanescent region is finite, and the energy leaking through the evanescent gap has to be included in the amplitude transmission coefficient.[27]

If the effective amplitude transmission coefficient is introduced into Eq. (42), the effective power transmission coefficient as given in Eq. (37) is obtained.

E. Density of Modes

The resonance condition, Eq. (12), links the mode number, the mode order, and the size parameter. Knowing that in the transition region ($\Lambda = x$) the internal rays hit the sphere's inner surface with the critical angle, and thus $\delta_B = 0$, one can derive an approximate expression for the number ν_{trans} of sharp ($x < \Lambda$) resonances of the lth multipole. Using Eq. (13), one finds that

$$\nu_{trans} = \frac{\Lambda}{\pi}\left[(n^2 - 1)^{1/2} - \arccos\left(\frac{1}{n}\right)\right] + \frac{3}{4}. \tag{46}$$

Now it is important to realize that the above relation may also be understood in the following way: In an interval of width Δx_ν [as given in Eq. (29)] every multipole will peak one time for each polarization; the sharpest resonances that one can find in this interval are the $TE_{l\approx nx,1}$ and $TM_{l\approx nx,1}$, respectively. The broadest ones, which are still narrow enough to be resolved, are the $TE_{l\approx x,\nu_{trans}}$ and $TM_{l\approx x,\nu_{trans}}$. This can readily be seen in Fig. 6, where the positions of all 131 TE resonances in the interval $100 < x < 110$ are shown as diamonds in (x, l) space. Resonances of identical mode order ν appear to lie on straight lines (labeled by the respective value of ν at the right edge

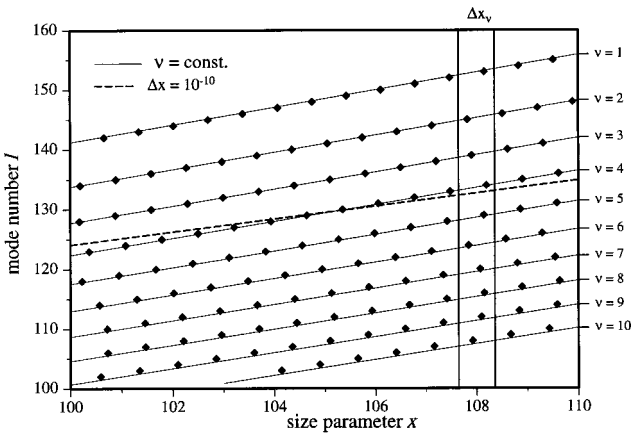

Fig. 6. Positions of 131 TE resonances in x, l space indicated by diamonds. The vertical lines enclose an interval of width Δx_ν. In total a number of $\nu_{\text{trans}}(=10)$ sharp ($x < \Lambda$) resonances can be found in this interval. There are $\nu_{\text{trans}} - \nu_{\Delta x}(=10 - 4 = 6)$ resonances in this interval that are broader than 10^{-10}; the line of constant resonance widths is indicated by the dashed line. This diagram serves to make visible the strategy for deriving Eq. (53).

of Fig. 6). The vertical lines enclose an interval of width Δx_ν around the arbitrarily chosen value of the size parameter $x = 108$.

Thus the number N of resonances in the mentioned interval is given by

$$N \approx 2\,\frac{x}{\pi}[(n^2 - 1)^{1/2} - \arctan(n^2 - 1)^{1/2}], \quad (47)$$

where we have expressed the across function in Eq. (46) by the arctan function, neglected the 3/4, and multiplied by 2 to account for the two possible states of polarization. If expression (47) is divided by the interval width Δx_ν, one obtains an expression for the density of modes. If we use Eq. (29) for the case $x \approx \Lambda$, which is justified since the resonance distance changes only slightly with varying mode order, one obtains

$$\frac{\mathrm{d}N_{\text{tot}}}{\mathrm{d}x} = x\,0.416(n^2 - 1)^{1/2}(n - 1), \quad (48)$$

where we replaced $[(n^2 - 1)^{1/2}/\arctan(n^2 - 1)^{1/2} - 1] \approx 0.653(n - 1)$. This is an excellent approximation for $1 < n < 2$. Equation (48) gives the mode density for all theoretically possible modes with $x < \Lambda$. However, very narrow resonances are often not observable in practice. Hence it is desirable to have an expression for the number of modes per size parameter interval that are likely to be found experimentally. To derive such an equation we recall two expressions that were found by the authors earlier[25]:

$$l \approx (nx) - (nx)^{1/3}\,\frac{1}{2}\left[3\left(\nu - \frac{1}{4}\right)\pi\right]^{2/3}, \quad (49)$$

$$l \approx x + x^{1/3}\,\frac{1}{2}\left[\frac{3}{2}\ln\left(\frac{\Delta x_{\text{trans}}}{\Delta x}\right)\right]^{2/3}. \quad (50)$$

The first relates the mode number and the size parameter to the mode order and follows from the resonance condition, Eq. (12). The second relates the mode number and the size parameter to the resonance with Δx; this expression follows from Eq. (38). An expression for the linewidth of resonances in the transition region Δx_{trans} was given in Eq. (40). Expression (49) was used to calculate the thin solid lines in Fig. 6, which trace the lines of constant mode order ν. Expression (50) was used to compute the dashed line, which, for given l, indicates the size parameter of resonances with constant linewidth of $\Delta x = 10^{-10}$. In the paper mentioned above,[25] more details about and the derivation of the above formulas may be found.

Expressions (49) and (50) can be used to eliminate l. If the resulting expression is solved for ν, one obtains

$$\nu_{\Delta x} = \frac{x}{\pi}\left[\frac{8}{9}\,\frac{(n-1)^3}{n}\right]^{1/2}\left(1 - \frac{1}{2(n-1)} \times \left\{\frac{3[\ln(\Delta x_{\text{trans}}) - \ln(\Delta x)]}{2x}\right\}^{2/3}\right)^{3/2} + \frac{1}{4}. \quad (51)$$

This equation gives the order of a resonance, once its theoretical width is known. For example, if $x = 108$ and $n = 1.5$ are introduced into Eq. (51), the result is $\nu_{\Delta x} = 4.03$ for $\Delta x = 10^{-10}$. For comparison, the $\text{TE}_{134,4}$ resonance at $x \approx 108.1751$ has a width of 3.61×10^{-11}.

Of course, it is not reasonable to use Eq. (51) if the rays are not totally internal reflected, that is, with values of Δx that are larger than Δx_{trans}, i.e., for resonances with $\Lambda < x$. However, for $\Delta x = \Delta x_{\text{trans}}$, Eq. (51) reads

$$\nu_{\text{trans}} = \frac{x}{\pi}\left[\frac{8}{9}\,\frac{(n-1)^3}{n}\right]^{1/2} + \frac{1}{4}, \quad (52)$$

which again is an expression for the mode order of resonances in the transition, i.e., $\Lambda \approx x$. For example, the resonance $\text{TE}_{128,12}$ with $n = 1.5$ is located at $x \approx 128.419 \approx \Lambda$. Equation (46) yields in this case $\nu_{\text{trans}} = 12.08$, whereas Eq. (52) yields $\nu_{\text{trans}} = 11.38$. Of course, it is also not reasonable to use Eq. (51) with resonance widths that are smaller than that of a first-order resonance. For example, the $\text{TE}_{112,1}$ resonance for a refractive index of 1.5 is located at $x \approx 80.1758$ and has a width of 5×10^{-17}. If these values are introduced into Eq. (51), the result is $0.985 \approx 1$, which shows the surprisingly high accuracy of Eq. (51).

Obviously, the difference between ν_{trans} (Eq. 52) and $\nu_{\Delta x}$ (Eq. 51) is the number of modes of different order that are broader than Δx. If we replace the term in front of the bold parentheses in Eq. (51), which represents ν_{trans}, by Eq. (46), multiply by the factor 2 to account for the two different states of polarization, and divide by the mode distance Δx_ν, we find the expression

$$\frac{\mathrm{d}N_\epsilon}{\mathrm{d}x} = \frac{\mathrm{d}N_{\text{tot}}}{\mathrm{d}x}F_\epsilon \quad (53)$$

for the density of modes with $\Delta x > \epsilon$, where

$$F_\epsilon = 1 - \left(1 - \frac{1}{2(n-1)}\left\{\frac{3[\ln(\Delta x_{\text{trans}}) - \ln(\epsilon)]}{2x}\right\}^{2/3}\right)^{3/2}. \quad (54)$$

To check the validity of this expression we compared the results with data given in the literature. Figure 7

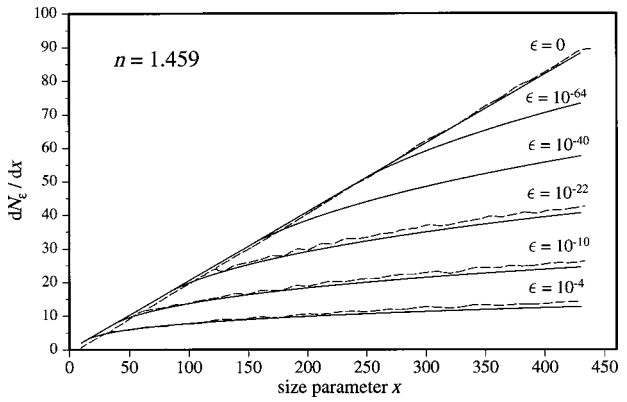

Fig. 7. Number of resonances per size parameter interval that are broader than ϵ. Comparison of our predictions (solid curves) with data from the literature (dashed curves) for different values of ϵ. The graph with $\epsilon = 0$ presents the total mode density; i.e., it takes all resonances into account.

shows plots of the total mode density [$\epsilon = 0$, Eq. (48)] as a function of the size parameter and for the density of modes with $\Delta x > \epsilon$ for five different values of ϵ (solid curves). The dashed curves represent data taken from the literature.[2] Taking into account the large number of approximations made in the course of the derivation of Eq. (53), the agreement between our expression and the numerically determined data is conincing. The error depends on the size parameter interval of interest but is always below 10%. Thus the accuracy of Eq. (53) should be satisfactory for most applications.

6. CONCLUSION

In the literature it is frequently stated that a resonance is a state where a ray after several round trips and surface reflections hits its tail in phase, i.e., a state where the length of the polygon-shaped ray path along one cavity round trip is an integer multiple of the internal wavelength. The discussion in the context of Fig. 2 clearly shows that the cavity round trip does not play any role; the only period of physical significance is the *radial* round trip. We showed that this conceptually and mathematically simple model is capable of providing physical insight and may be used to derive several approximate expressions for various quantities of practical interest.

Address correspondence to G. Roll at roll@lat2.lat.ruhr-uni-bochum.de.

REFERENCES AND NOTES

1. C. F. Bohren and D. R. Huffman, *Absorption and Scattering of Light by Small Particles* (Wiley, New York, 1983).
2. S. C. Hill and R. E. Benner, "Morphology-dependant resonances," in *Optical Effects Associated with Small Particles*, P. W. Barber and R. K. Chang, eds. (World Scientific, Singapore, 1988).
3. R. K. Chang and A. J. Campillo, eds., *Optical Processes in Microcavities* (World Scientific, Singapore, 1996).
4. S. C. Hill and R. K. Chang, "Nonlinear optics in droplets," in *Studies in Classical and Quantum Nonlinear Optics*, O. Keller, ed. (Nova Science, New York, 1995).
5. H. B. Lin and A. J. Campillo, "Radial profiling of microdroplets using cavity-enhanced Raman spectroscopy," Opt. Lett. **20**, 1589–1591 (1995).
6. T. Kaiser, G. Roll, and G. Schweiger, "Investigation of coated droplets in an optical trap: Raman scattering, elastic light scattering and evaporation characteristics," Appl. Opt. **35**, 5918–5924 (1996).
7. J. L. Huckaby, A. K. Ray, and B. Das, "Determination of size, refractive index, and dispersion of single droplets from wavelength-dependent scattering spectra," Appl. Opt. **33**, 7112–7125 (1994).
8. G. Chen, M. M. Mazumder, R. K. Chang, J. C. Swindal, and W. P. Acker, "Laser diagnostics for droplet characterization: application of morphology dependent resonances," Prog. Energy Combust. Sci. **22**, 163–188 (1996).
9. J. B. Keller and S. I. Rubinow, "Asymptotic solution of eigenvalue problems," Ann. Phys. (New York) **9**, 24–75 (1960).
10. S. J. Maurer and L. B. Felsen, "Ray-optical techniques for guided waves," Proc. IEEE **55**, 1718–1729 (1967).
11. G. Roll, T. Kaiser, S. Lange, and G. Schweiger, "Ray interpretation of multipole fields in spherical dielectric cavities," J. Opt. Soc. Am. A **15**, 2879–2891 (1998).
12. G. Roll, T. Kaiser, and G. Schweiger, "Eigenmodes of spherical dielectric cavities: coupling of internal and external rays," J. Opt. Soc. Am. A **16**, 882–895 (1999).
13. J. D. Jackson, *Classical Electrodynamics* (Wiley, New York, 1975).
14. This statement holds only for light with the frequency of the illuminating plane wave; secondary fields, e.g., excited Raman or fluorescence fields, are not restricted to modes with azimuthal mode number $m = 1$.
15. M. Born and E. Wolf, *Principles of Optics* (Pergamon, Oxford, UK, 1993).
16. Throughout this paper we mean the trigonometric expansions of Bessel functions [compare expressions (18) and (19)] when we use the term Debye expansion. This must not be confused with the Debye series expansion of the scattering coefficients of Mie theory. Both the Debye expansion of Bessel functions and the Debye series expansion of the Mie coefficients play an important role in the ray description of the interaction of light with dielectric spheres. The former expansions are approximations to the exact functions, which break down in regions where the argument approaches the order. These expansions are found when the field within an illuminated sphere is investigated by means of geometrical optics.[11] The Debye series expansion, on the other hand, denotes a mathematically exact technique to formulate the scattering process in terms of surface interactions of multipole waves. The Debye series expansion is equivalent to Mie theory but shows many similarities to the multiple-interference description of geometrical optics.[17]
17. J. A. Lock, "Cooperative effects among partial waves in Mie scattering," J. Opt. Soc. Am. A **5**, 2032–2044 (1988).
18. N. S. Kapany and J. J. Burke, *Optical Waveguides* (Academic, London, 1972), p. 126.
19. P. Chýlek, "Resonance structure of Mie scattering: distance between resonances," J. Opt. Soc. Am. A **7**, 1609–1613 (1990).
20. J. R. Probert-Jones, "Resonance component of backscattering by large dielectric spheres," J. Opt. Soc. Am. A **1**, 822–830 (1984).
21. P. M. Aker, P. A. Moortgat, and J. X. Zhang, "Morphology-dependent stimulated Raman scattering imaging. I. Theoretical aspects," J. Chem. Phys. **105**, 7268–7275 (1996).
22. C. C. Lam, P. T. Leung, and K. Young, "Explicit asymptotic formulas for the positions, widths, and strength of resonances in Mie scattering," J. Opt. Soc. Am. B **9**, 1585–1592 (1992).
23. B. R. Johnson, "Theory of morphology-dependent resonances: shape resonances and width formulas," J. Opt. Soc. Am. A **10**, 343–352 (1993).
24. At first glance this may be surprising, since we always assumed the rays to be confined by total internal reflection,

which should mean $T = 0$. However, owing to the curved surface, the energy confinement is not perfect, but there is a so-called evanescent leakage. Consequently the energy loss—although small—is not zero.
25. G. Roll, T. Kaiser, and G. Schweiger, "Controlled modification of the expansion order as a tool in Mie computations," Appl. Opt. **37**, 2483–2492 (1998).
26. The fact that the transmission coefficient t is complex in the case of total reflection indicates the fact that the evanescent field is phase shifted with respect to the incident wave. The phase shift is half as large as that of the reflected wave.
27. A. W. Snyder and J. D. Love, *Optical Waveguide Theory* (Chapman & Hall, London, 1983).